RESEARCH PAPER

Behavioral Control for Multiple Omnidirectional Mobile Robots via Fully Actuated System Approach

Zhibin Mo[a], Wanquan Liu[a], Yu-Yao Wu[a], Hui-Jie Sun[a]

[a] Shenzhen Campus of Sun Yat-sen University, Shenzhen 518107, Guangdong, China

ARTICLE HISTORY
Compiled December 18, 2024

ABSTRACT

In this paper, the collision-free formation control issue is investigated for a group of omnidirectional mobile robots with uncertain dynamics and external disturbances. To address this, a fully actuated behavioral control scheme is proposed by integrating the fully actuated system theory into the null-space-based behavioral control method. First, three distributed formation behaviors are developed by transforming the behavioral functions into a fully actuated configuration. Then, the asymptotic stability of these three behaviors and their null-space-based projection fusion are established using Lyapunov theory. Furthermore, a fully actuated sliding mode controller is designed for the over-actuated omnidirectional mobile robots to ensure asymptotic convergence at the dynamic level, thereby enabling the precise tracking of desired kinematic commands in the task space under model uncertainty. Finally, simulation results are provided to demonstrate that the closed-loop system is asymptotically stable, revealing the effectiveness of the proposed scheme. To ensure the repeatability, our codes are available on Github:https://github.com/EzekielMok/Fully-Actuated-Behavioral-Control.git.

KEYWORDS
Omnidirectional mobile robots, fully actuated theory, null-space-based behavioral control, formation control, collision avoidance.

1. Introduction

Recently, mobile robots are extensively used in both civilian and military applications due to their enhanced mobility and greater flexibility. As an indispensable component of mobile robots, the omnidirectional mobile robot (OMR) (Taheri & Zhao, 2020) has been gaining popularity in a variety of applications, particularly in environments with limited space and high demands for maneuverability, such as warehouses (Bayar & Ozturk, 2020; Costa et al., 2016), hospitals (Guo, Yee, Mun, & Yu, 2017; Takahashi, Suzuki, Shitamoto, Moriguchi, & Yoshida, 2010), rescue (Jin, Wang, Zhao, & Yu, 2022), logistics (Thanh, Long, Ly, Thai, & Thien, 2023) and factories (Giurgiu, Bârsan, Virca, & Pupăză, 2022). They are often organized into groups to perform parallel, cooperative, or even conflicting control tasks and objectives, such as distributed formation, collision avoidance, individual mission execution, and more. Such configurations are known as multiple omnidirectional mobile robot systems (Multi-OMRs).

A key focus of research on Multi-OMRs is solving the formation tracking control

CONTACT Hui-Jie Sun, Email: sunhj6@mail.sysu.edu.cn

problem, which aims to efficiently guide robots to assemble and maintain a desired formation. On the one hand, the special wheel characteristics are conducive to broadening its application prospects in cooperative tasks. On the other hand, the structural complexity poses great challenges to the development of consensus control algorithms, like the formation control problems under model uncertainty and external disturbances, which is still deserve in-depth study.

Extensive research has been conducted on developing distributed and cooperative controllers for Multi-OMR. Specifically, in (Yu, Chen, & Xu, 2021), a fuzzy logic-based distributed consensus strategy was proposed for the self-organizing formation control task of Multi-OMRs. In (Wang et al., 2022), the model predictive control-based method was applied to the formation control of Multi-OMRs with physical constraints and model uncertainty. In (Xiao, Yu, & Chen, 2022), a distributed consensus protocol was proposed for the self-triggered organization formation control of Multi-OMRs. In (Jin et al., 2022), an incremental updating method based on a second-order communication topology was proposed for solving the formation control problem of large-scale Multi-OMRs. In (Eyuboglu & Atali, 2023), a novel obstacle detection method based on collaborative path planning was proposed for the formation control of Multi-OMRs.

However, previous research has successfully achieved efficient formation control for Multi-OMRs, the critical issue of conflict resolution in cooperative formation tasks remains largely unexplored. Conflicts among OMRs are inevitable during the execution of cooperative tasks Zhou, Cheng, Sun, & Xia (2022), making it a persistent challenge to regulate Multi-OMRs for achieving distributed formation, especially under the constraints of multi-task conflicts. The null-space-based behavioral control approach (Baizid, Giglio, Pierri, Trujillo, & Antonelli, 2017) offers an effective approach to addressing the conflict resolution problem in Multi-OMR formation control. Within the NSBC scheme, control objectives are hierarchically structured into multiple tasks, ensuring that higher-priority tasks are executed first, while lower-priority tasks are executed only after being projected into the null space of higher-priority tasks. Over the past few decades, various modeling approaches have been explored to design distributed behavioral control methods. For instance, a distributed NSBC algorithm was developed in (Tan et al., 2022), where mobile robots are divided into smaller, fully connected subgroups restricted to static formations. In (Matouš, Pettersen, Varagnolo, & Paliotta, 2024), a distributed NSBC algorithm was introduced to enable formation path-following for systems of multiple autonomous mobile robots. A fixed-time behavioral control strategy addressing time-varying formation control with collision constraints was proposed in (Zheng et al., 2023). In (Zhou, Cheng, Xia, & Liu, 2020) and (Zhou et al., 2022), a distributed fixed-time estimator for directed spanning tree communication topologies was presented, along with a distributed fixed-time behavioral strategy at the kinematic level. This approach achieves fixed-time collaborative behavioral control for multi-agent systems with second-order nonlinear dynamics.

The cooperative control methods mentioned above both achieve precise formation tracking for Multi-OMRs or multi-agent systems. However, they are all model-based methods that require an accurate system model. Moreover, the strong system nonlinearity and model uncertainty make the global stabilization problem for Multi-OMRs particularly challenging (Duan, 2021a,b,c) . As a result, designing cooperative controllers faces numerous difficulties, including complex structures, numerous parameters, a lack of physical interpretation, and stringent stability requirements. Therefore, in recent years, scholars have proposed a high-order fully actuated control theory approach for nonlinear systems (Duan, 2024; Duan, Zhou, & Yang, 2024; Wu, Zhou, Hou, & Zhang, 2022). This method involves a fully actuated transformation and the

design of a feedback linearization controller, optimizing control efficiency and stability through a simplified linear closed-loop system. In (Duan, 2024), the author proposed that many nonlinear systems can either be physically modeled as high-order fully actuated systems or transformed into them. The concept of full actuation can be extended to develop high-order fully actuated models, which have the potential to describe a wide range of practical and theoretical systems (Duan, 2021d). These models leverage the fully actuated characteristic to simplify control solutions, making them more efficient and effective. The properties of fully actuated systems ensure that control variables can be obtained analytically, providing significant convenience in the control of general nonlinear systems.

It is noted our previous work (Mo, Liu, Wu, & Sun, 2024) has attempted to explore the fully actuated behavioral control for Multi-OMRs, which only focused on fully actuated attribute and the convergence of the behavioral tracking error, while the fully actuated attribute and the convergence in task space were not considered.

Motivated by the discussions mentioned above, a novel fully actuated behavioral control scheme is designed to achieve the desired distributed formation control for Multi-OMRs. The innovation of this work involves the following aspects. First, this work refines the behavioral control theory by introducing the fully actuated system approach to the design of behaviors and behavioral controllers , which is the theoretical innovation of this work. Moreover, the fully actuated behavior is discussed for the first time at the behavioral task-space error level of Multi-OMRs, which is the practical innovation of this work in terms of research problems. The main contributions are summarized as follows.

(1) Three distributed fully-actuated formation behaviors are developed by transforming the behavioral functions into a fully-actuated configuration to solve the admissible and desired velocity collision-free formation planning.
(2) A fully-actuated sliding mode controller is designed for the over-actuated system model to ensure asymptotic convergence at the dynamic level, enabling precise tracking of the planned formation.

The rest of this paper is structured as follows. Section 2 introduces the preliminaries and problem statement. Section 3 presents the proposed fully actuated behavioral control for Multi-OMRs. Section 4 covers several numeral simulation results. Finally, Section 5 concludes this paper.

Notation 1. Given a vector $\boldsymbol{a} = [a_1, a_2, a_3]^\top$, the function $\text{sig}^r(\boldsymbol{a})$ is in the form of $\text{sig}^r(\boldsymbol{a}) = [|a_1|^r\text{sign}(a_1), |a_2|^r\text{sign}(a_2), |a_3|^r\text{sign}(a_3)]^\top$, where $|\cdot|$ is the operator of absolute value, $\text{sign}(\cdot)$ represents a standard sign function, r is positive constant. Let $\overline{\lambda}(\cdot), \underline{\lambda}(\cdot)$ denote the maximum and minimum eigenvalue value, respectively. Denote the $\|\cdot\|$ as $L2$ norm of a vector or matrix. And the behavior can also be named mission or task in behavioral control in this study.

2. Problem Statement and Preliminaries

This paper investigates the OMRs equipped with four mecanum wheels, which perform excellent mobility and greater flexibility in limited spaces, as shown in Fig. 1(a). The primary control objective is to enable a group of OMRs to maintain a distributed formation while effectively avoiding collisions. Each OMR is equipped with a decision-making computing unit, allowing them to perform cooperative and parallel tasks

through a distributed communication network. To achieve this, the system dynamic modeling process is essential. Therefore, the dynamic model of OMR is given as follow.

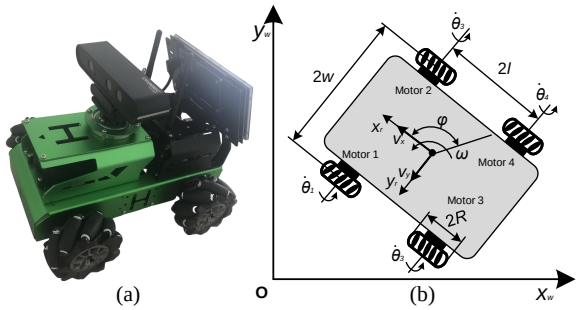

Figure 1. (a) The lateral view of the prototype. (b) The coordinate frames of the OMR.

2.1. System Dynamic Modeling

To accurately model the translational and rotational motion of the OMR, it is assumed that all OMRs are constrained to move on a flat and horizontal plane such that the wheels experience no slippage in the direction of the traction force.

As shown in Fig. 1(b), the world coordinate frame $x_{\mathrm{w}}o_{\mathrm{w}}y_{\mathrm{w}}$ is fixed on the ground from the original point, and the robotic moving coordinate frame $x_{\mathrm{r}}o_{\mathrm{r}}y_{\mathrm{r}}$ established on

Table 1. VARIABLES AND PARAMETERS NOMENCLATURE

Symbols	Definitions
$\boldsymbol{q} = [x_{\mathrm{r}}, y_{\mathrm{r}}, \varphi]^{\top}$	The position and orientation angle in the world coordinate frame;
$\boldsymbol{v}_{\mathrm{w}} = [\dot{x}_{\mathrm{w}}, \dot{y}_{\mathrm{w}}, \dot{\varphi}]^{\top}$	The transnational and rotational velocity in the world coordinate frame;
$\boldsymbol{v}_{\mathrm{r}} = [\dot{x}_{\mathrm{r}}, \dot{y}_{\mathrm{r}}, \dot{\varphi}]^{\top}$	The transnational and rotational velocity in the moving coordinate frame;
$\dot{\boldsymbol{\theta}} = \left[\dot{\theta}_1, \dot{\theta}_2, \dot{\theta}_3, \dot{\theta}_4\right]^{\top}$	The angular velocity of four driving motors;
$\boldsymbol{u} = \left[\tau_1, \tau_2, \tau_3, \tau_4\right]^{\top}$	The control input of the OMR;
m	The Multi-OMRs of robot;
w	Half of the tread length;
l	Half of the wheelbase length;
R	The radius of wheels;
C_{f}	The static friction;
C_{θ}	The viscous friction coefficient;
$\boldsymbol{h}_{\mathrm{d}}$	The model uncertainty;
I_{z}	The moment of inertia around the z axle in the moving coordinate frame;
I_{w}	The moment of inertia of wheels around the wheel axle.

the geometric center of the OMR. The definitions of variables and parameters related to system dynamic modeling are defined in Table 1.

By applying the geometric relationship described in Fig. 1 (b), the kinematic mapping of the state between robotic moving coordinate frame and the motor angular space can be expressed by

$$\boldsymbol{v}_{\mathrm{r}} = R\boldsymbol{P}^{\dagger}\dot{\boldsymbol{\theta}}, \tag{1}$$

where $\boldsymbol{P}^{\dagger} = \boldsymbol{P}^{\top}(\boldsymbol{P}\boldsymbol{P}^{\top})^{-1}$ is the pseudo-inverse of $\boldsymbol{P}$, and

$$\boldsymbol{P} = \begin{bmatrix} 1 & -1 & -(l+w) \\ 1 & 1 & (l+w) \\ 1 & 1 & -(l+w) \\ 1 & -1 & (l+w) \end{bmatrix}. \tag{2}$$

Thus, the velocity described in world coordinate frame can be obtained by $\boldsymbol{v}_{\mathrm{w}} = \boldsymbol{T}(\varphi)\,\boldsymbol{v}_{\mathrm{r}}$, where the rotation matrix can be defined as

$$\boldsymbol{T}(\varphi) = \begin{bmatrix} \cos(\varphi) & -\sin(\varphi) & 0 \\ \sin(\varphi) & \cos(\varphi) & 0 \\ 0 & 0 & 1 \end{bmatrix}. \tag{3}$$

Using the Euler-Lagrange method (Yu et al., 2021), the second order nonlinear dynamic equation of OMR can be formulated as

$$\ddot{\boldsymbol{q}} + \boldsymbol{A}_0\dot{\boldsymbol{q}} + \boldsymbol{A}_1 - \boldsymbol{d} = \boldsymbol{B}\boldsymbol{u}, \tag{4}$$

where
$\boldsymbol{A}_0 = \boldsymbol{T}(\varphi)\,\dot{\boldsymbol{T}}^{-1}(\varphi) + C_\theta R^2 \boldsymbol{T}(\varphi)\,\boldsymbol{P}^{\dagger}\boldsymbol{M}^{-1}\boldsymbol{P}\boldsymbol{T}^{-1}(\varphi)$, $\boldsymbol{A}_1 = R^2\boldsymbol{T}(\varphi)\,\boldsymbol{P}^{\dagger}\boldsymbol{M}^{-1}C_{\mathrm{f}}mg$,
$\boldsymbol{B} = R\boldsymbol{T}(\varphi)\,\boldsymbol{P}^{\dagger}\boldsymbol{M}^{-1}$, $\boldsymbol{d} = R\boldsymbol{T}(\varphi)\,\boldsymbol{P}^{\dagger}\boldsymbol{M}^{-1}\boldsymbol{h}_{\mathrm{d}}$,

$$\boldsymbol{M} = \begin{bmatrix} M_3 & -M_2 & M_2 & M_4 \\ -M_2 & M_3 & M_4 & M_2 \\ M_2 & M_4 & M_3 & -M_2 \\ M_4 & M_2 & -M_2 & M_3 \end{bmatrix},$$

and $M_1 = \frac{mR^2}{8}$, $M_2 = \frac{I_z R^2}{16(l+w)^2}$, $M_3 = M_1 + M_2 + I_{\mathrm{w}}$, $M_4 = M_1 - M_2$, g denotes the gravitational acceleration.

The distributed formation task guides the OMRs toward their desired reference positions and velocities. To facilitate this, the reference signal $\boldsymbol{q}_{\mathrm{d}}$ is introduced to establish the error dynamics of the OMR. Define the tracking error as $\boldsymbol{e}_i = \boldsymbol{q}_i - \boldsymbol{q}_{\mathrm{d}}$. Thus, the error dynamic equation of OMR that illustrated in Fig. 1(a) is written as

$$\ddot{\boldsymbol{e}} + \ddot{\boldsymbol{q}}_{\mathrm{d}} + \boldsymbol{A}_1 + \boldsymbol{A}_0\dot{\boldsymbol{e}} + \boldsymbol{A}_0\dot{\boldsymbol{q}}_{\mathrm{d}} - \boldsymbol{d} = \boldsymbol{B}\boldsymbol{u}, \tag{5}$$

where $\dot{\boldsymbol{e}}, \dot{\boldsymbol{q}}_{\mathrm{d}}$ are the first derivative of $\boldsymbol{e}$ and $\boldsymbol{q}_{\mathrm{d}}$, respectively. $\ddot{\boldsymbol{e}}$ and $\ddot{\boldsymbol{q}}_{\mathrm{d}}$ are their second derivative. The singular model of the OMR is then utilized to construct the Multi-OMRs model.

Consider a Multi-OMRs consisting of n OMRs, the index $i \in \{1, 2, \cdots, n\}$ denotes i^{th} robot. Based on the singular model of OMR in (5), the dynamic equation of i^{th}

robot in Multi-OMRs can be obtained as

$$\ddot{\boldsymbol{e}}_i + \ddot{\boldsymbol{q}}_{\mathrm{d},i} + \boldsymbol{A}_1 + \boldsymbol{A}_0\dot{\boldsymbol{e}}_i + \boldsymbol{A}_0\dot{\boldsymbol{q}}_{\mathrm{d},i} - \boldsymbol{d}_i = \boldsymbol{B}\boldsymbol{u}_i, \tag{6}$$

The established dynamic model (6) of the Multi-OMRs will be utilized to control each OMR in executing the distributed formation task. Therefore, the preliminary of algebraic graph must be provided to describe the relationship among n OMR before developing the specific behavioral control scheme.

2.2. Algebraic Graph Theory

By using the algebraic graph theory (Huang, 2024), the coupling relationships of the communication network among n robot can be characterized by a directed weighted graph $\boldsymbol{\mathcal{G}}_1 = \{\boldsymbol{V}, \boldsymbol{\varsigma}, \boldsymbol{\mathcal{A}}\}$, where $\boldsymbol{V} = \{v_1, v_2, \ldots, v_n\}$ denotes the node set, $\boldsymbol{\varsigma} = \{(v_i, v_j) : v_i, v_j \in \boldsymbol{V}, i \neq j\}$ represents a set composed of edges, and matrix $\boldsymbol{\mathcal{A}} = [a_{ij}] \in \mathbb{R}^{n\times n}$ is a weighted adjacency matrix of graph $\boldsymbol{\mathcal{G}}_1$, where the symbol of a_{ij} denotes the direction of signal transmission, and the magnitude of its absolute value represents communication strength between i^{th} robot and j^{th} robot. Then, define $\boldsymbol{\mathcal{G}}_0$ as the directed weighted graph of virtual leader. The $\boldsymbol{\mathcal{B}} = [b_1, \cdots, b_n] \in \mathbb{R}^n$ denotes the leader adjacency matrix of $\boldsymbol{\mathcal{G}}_0$ and $\boldsymbol{\mathcal{G}}_1$. In a directed graph, if there exists a node with a directed path to any other node, it is called directed spanning tree.

For the rigor of theoretical deduction, necessary assumptions are enumerated.

Assumption 2.1. *In this paper, the trajectory (position $\boldsymbol{q}_0$ and velocity $\boldsymbol{v}_0$) of the virtual leader required to be bounded, which is assumed that $|\boldsymbol{q}_0| \leq \chi_1$ and $|\boldsymbol{v}_0| \leq \chi_2, \forall t \in [0, +\infty)$, for two given constant χ_1 and χ_2, respectively.*

Assumption 2.2. *The communication network graph $\boldsymbol{\mathcal{G}} = \{\boldsymbol{\mathcal{G}}_0, \boldsymbol{\mathcal{G}}_1\}$ is assumed to be a fixed and directed spanning tree.*

2.3. Fully Actuated Control Theory

Consider the nonlinear system

$$\boldsymbol{E}\boldsymbol{x} = g(\boldsymbol{x}^{(0\sim m-1)}, t) + \boldsymbol{B}(\boldsymbol{x}^{(0\sim m-1)}, t))\boldsymbol{u}, \tag{7}$$

where $m > 0$ is a constant to defined the order of the system, $\boldsymbol{x}(t) \in \mathbb{R}^n$ denotes the state vector of the system. $\boldsymbol{u} \in \mathbb{R}$ represents the input vector of the system. $g(\boldsymbol{x}^{(0\sim m-1)}, t) \in \mathbb{R}$ is a continuous vector function. $\boldsymbol{E} \in \mathbb{R}^{n\times n}$ denotes the inertia matrix, which can be singular. And $\boldsymbol{B}(\boldsymbol{x}^{(0\sim m-1)}, t)) \in \mathbb{R}^{n\times n}$ represents the input coefficient matrix, $\boldsymbol{x}^{(0\sim m-1)} = [\boldsymbol{x}, \dot{\boldsymbol{x}}, \ldots, \boldsymbol{x}^{(m-1)}]^\top$. Then, the definition and necessary Lemma of the fully actuated control system (12) can be derived, as shown below.

Definition 2.3. (Duan, 2024)). For any $\boldsymbol{x} \in \mathbb{R}$, $t > 0$, if the $\boldsymbol{B}(\boldsymbol{x}^{(0\sim m-1)}, t))$ is non-singular, then the system (7) can be defined as a fully actuated control system.

Lemma 2.4. *(Duan, 2024)). For a fully actuated system* (7)*, define $\boldsymbol{A}_{(0\sim m-1)} = [\boldsymbol{A}, \boldsymbol{A}_1, \ldots, \boldsymbol{A}_{m-1,}]$, where each $\boldsymbol{A}_i \in \mathbb{R}^{n\times n}$ represents the parameter matrices of the*

system (12)*, then the closed-loop control law can be designed as*

$$\begin{aligned}\boldsymbol{u} = &- \boldsymbol{B}^{-1}(\boldsymbol{x}^{(0\sim m-1)}, t))\big[\boldsymbol{A}_{(0\sim m-1)}\boldsymbol{x}^{(0\sim m-1)} \\ &+ g(\boldsymbol{x}^{(0\sim m-1)}, t) - \boldsymbol{\Gamma}_0\big],\end{aligned} \tag{8}$$

where $\boldsymbol{\Gamma}_0 \in \mathbb{R}^n$ *is the external control term to be designed.*

2.4. Null-space-based behavioral control

The NSBC approach can be structured into three hierarchical levels: elementary behaviors, composite behaviors, and the task supervisor. This framework enables the task supervisor to derive reference velocity signals for the autonomous robots by hierarchically combining the velocity outputs of elementary behaviors using geometric principles. In the NSBC framework, elementary behaviors are the atomic task functions to be controlled at the kinematic level. They can be expressed by a function that involves the degree of freedom of the system and variables to be controlled.

For the elementary behaviors, define $\boldsymbol{\rho} \in \mathbb{R}^m$ as the task variable and $\boldsymbol{\delta} \in \mathbb{R}^n$ as the system configuration. $\boldsymbol{\rho}$ is the function related to $\boldsymbol{\delta} : \mathbb{R}^m \to \mathbb{R}^n$. Then, the corresponding behavioral task function of each robot can be expressed as

$$\boldsymbol{\rho}_i = f(\boldsymbol{\delta}_i). \tag{9}$$

The corresponding differential relationship of (9) is

$$\dot{\boldsymbol{\rho}}_i = \boldsymbol{J}_i(\boldsymbol{\delta}_i)\boldsymbol{v}_i, \tag{10}$$

where $\boldsymbol{J}_i(\boldsymbol{\delta}) = \frac{\partial f(\boldsymbol{\delta}_i)}{\partial \boldsymbol{\delta}_i} \in \mathbb{R}^{m\times n}$ is the configuration-related task Jacobian matrix of the i^{th} robot and $\boldsymbol{v}_i \in \mathbb{R}^n$ is the stacked vector of the i^{th} robot. n depends on the specific system and controllable degrees of freedom.

The system configuration is considered as the position and orientation. The reference velocity $\boldsymbol{v}_{\text{d}}$ can be calculated by converting the local linear mapping 10 into the least square formula. The integration of reference velocity would incur a certain drift of the reconstructed state, which can be compensated for by the closed loop inverse kinematics (CLIK) algorithm (Antonelli & Chiaverini, 2006):

$$\boldsymbol{v}_{\text{d},i} = \boldsymbol{J}_i^{\dagger}(\dot{\boldsymbol{\rho}}_{\text{d},i} + \boldsymbol{\Lambda}_i(\boldsymbol{\rho}_{\text{d},i} - \boldsymbol{\rho}_i)), \tag{11}$$

where $\boldsymbol{J}_i^{\dagger} = \boldsymbol{J}_i^{\top}(\boldsymbol{J}_i\boldsymbol{J}_i^{\top})^{-1}$ is the pseudo-inverse matrix of $\boldsymbol{J}_i(\boldsymbol{\delta}_i)$ and $\boldsymbol{\Lambda}_i$ is a gain matrix of positive-definite constant. Let $\boldsymbol{\rho}_{\text{d},i}, \boldsymbol{\rho}_i$ be the desired and actual task function value of the i^{th} robot, respectively. $\tilde{\boldsymbol{\rho}}_i = \boldsymbol{\rho}_{\text{d},i} - \boldsymbol{\rho}_i$ be the task error.

The system dynamics and preliminaries are then employed to design a fully actuated behavioral control scheme, addressing the challenge of collision-free formation control. It is important to highlight that the primary objective of this paper is to develop a distributed formation control scheme for nonlinear multi-agent systems (Multi-OMRs) as described by (1), such that the current state $\boldsymbol{x}_i(t)$ of each agent synchronizes closely with the corresponding distributed reference state $\boldsymbol{x}_{i,\text{r}}(t)$. The goal is for the formation tracking error $\boldsymbol{e}_i(t) = \boldsymbol{x}_i(t) - \boldsymbol{x}_{i,\text{r}}(t)$ to converge to a small residual set containing the origin (zero), and for the agents to maintain synchronization thereafter while avoiding

collisions. Then, the total formation control objectives are described as followed.

For any initial state $\boldsymbol{x}_i(t_0)$, there exist a controller $\boldsymbol{u}_i$, the system satisfy that

$$\begin{cases} \lim\limits_{t\to\infty} |\boldsymbol{x}_i(t) - \boldsymbol{x}_{i,\mathrm{r}}(t)| \leqslant c, \\ |\boldsymbol{x}_i(t) - \boldsymbol{x}_{\mathrm{o}}(t)| > D_{\mathrm{s}}, \forall t > 0, \end{cases} \tag{12}$$

where $\boldsymbol{x}_o(t)$ represents the total set of obstacle or other relevant robot, and c is a small and positive constant, D_{s} denotes the minimum safe distance.

3. Fully Actuated Distributed Behavioral Control Scheme Design

To achieve the control objective of collision-free distributed formation control for Multi-OMRs, this section details the design of a fully actuated behavioral control scheme, as illustrated in Figure 2. The proposed scheme is structured into three hierarchical levels: the kinematics level, the data processing level, and the dynamic level. Together, these levels form a closed-loop framework for decision-making and control, as represented by ① to ③ in the block diagram. Their applications and interrelations are summarized as follows:

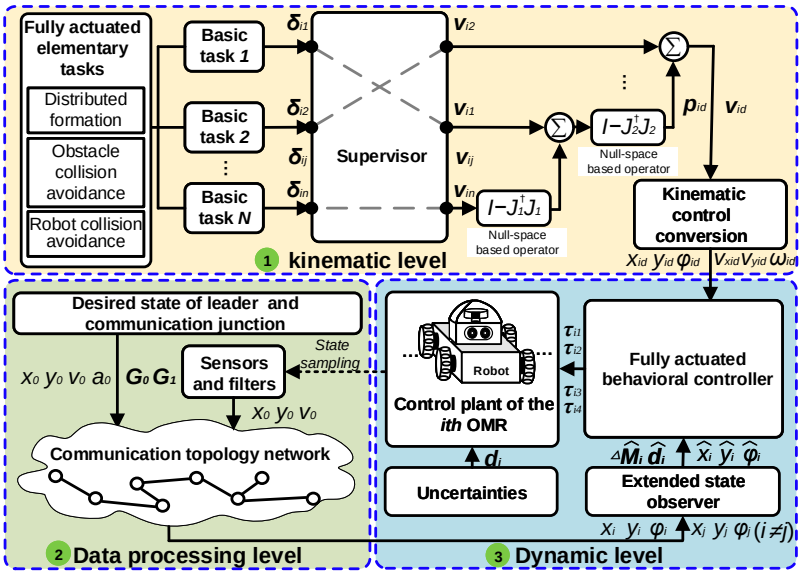

Figure 2. The overall scheme of the fully actuated behavioral control method.

(1) **Kinematic Level:** The designed fully actuated distributed behaviors at the kinematic level generate desired kinematic guidance (composite output) for the behavioral controller at the dynamic level.

(2) **Dynamic Level:** The fully actuated sliding mode controller designed at the dynamic level compensates for the nonlinear dynamics and uncertainty of the Multi-OMRs to track the composite output, while simultaneously uploading sensor sampling data to the data processing level.

(3) **Data Processing Level:** The distributed estimator at the data processing level uses sensor data to estimate the formation tracking reference, which is subsequently provided to the kinematic level.

3.1. Fully Actuated Distributed Behaviors

To address the collision-free formation control issue for Multi-OMRs, a virtual leader ($\boldsymbol{q}_0 = \left[x_0, y_0, \varphi_0\right]^\top$ and $\boldsymbol{v}_0 = \left[\dot{x}_0, \dot{y}_0, \dot{\varphi}_0\right]^\top$) is designated as the reference point, with each agent configured to maintain specific position $\boldsymbol{\varrho}$ and velocity offsets $\dot{\boldsymbol{\varrho}}$ relative to this leader. The affine image of the nominal configuration is then introduced to describe the time-varying configuration of the target formation, which is designed as

$$\boldsymbol{\varrho} = \left[\boldsymbol{\varrho}_1^\top, \cdots, \boldsymbol{\varrho}_n^\top\right]^\top = \left[I_n \otimes \boldsymbol{W}(t)\right] \boldsymbol{r} + \mathbf{1}_n \otimes \boldsymbol{b}(t), \tag{13}$$

where $I_n \in \mathbb{R}^{n\times n}$ is a identity matrix, $\mathbf{1}_n \in \mathbb{R}^n$ represent a vector of element 1. $\boldsymbol{r} = \left[\boldsymbol{r}_1^\top, \cdots, \boldsymbol{r}_n^\top\right]^\top \in \mathbb{R}^{dn}$ is a constant configuration of time-varying formation, and $\boldsymbol{W} \in \mathbb{R}^{d\times d}$ and $\boldsymbol{b}(t)$ are the continuous function of time t. $\otimes$ denotes a Kronecker product calculator. Then, the offset can be formulated as $\boldsymbol{\varrho}_i = \boldsymbol{W}(t)\boldsymbol{r}_i + \boldsymbol{b}(t)$.

The design of elementary behaviors is fundamental to the behavior control approach. In this section, the various tasks that can be performed by OMRs are examined. Considering the task requirements and actuator characteristics, this paper define three elementary behaviors: fully actuated distributed formation behavior (FDB), fully actuated obstacle collision avoidance behavior (FOCB), and the fully actuated robot collision avoidance behavior (FRCB).

3.1.1. Fully Actuated Distributed Formation Behavior

This part focuses on the distributed formation behavior, where all agents move toward achieving a predefined desired formation. In the distributed formation configuration, each robot cannot directly access the state of the leader or other robots. Instead, it can only communicate with its directed neighboring robots. Therefore, within a robot, the state of the virtual leader or other robots must be estimated using a so-called distributed estimator. Let $\hat{\boldsymbol{q}}_{0,i}$ and $\hat{\boldsymbol{v}}_{0,i}$ represent the distributed estimation of $\boldsymbol{p}_0$ in the i^{th} OMR, which can be obtained within a fixed time under *Assumption 2.2* and *Assumption 2.2* using a distributed estimator:

$$\begin{cases} \dot{\hat{\boldsymbol{q}}}_{0,i} = -\iota_1 \mathrm{sig}^{\eta_1}\left(\hat{\boldsymbol{e}}_{q0}\right) - \iota_2 \mathrm{sign}\left(\hat{\boldsymbol{e}}_{q0}\right) + \hat{\boldsymbol{v}}_{0,i}, \\ \dot{\hat{\boldsymbol{v}}}_{0,i} = -\iota_3 \mathrm{sig}^{\eta_2}\left(\hat{\boldsymbol{e}}_{v0}\right) - \iota_4 \mathrm{sign}\left(\hat{\boldsymbol{e}}_{v0}\right), \end{cases} \tag{14}$$

where $\hat{\boldsymbol{e}}_{q0} = \sum_{j=1}^{n} a_{ij}(\hat{\boldsymbol{q}}_{0,i} - \hat{\boldsymbol{q}}_{0,j}) + b_i(\hat{\boldsymbol{q}}_{0,i} - \boldsymbol{q}_0)$ and $\hat{\boldsymbol{e}}_{v0} = \sum_{j=1}^{n} a_{ij}(\hat{\boldsymbol{v}}_{0,i} - \hat{\boldsymbol{v}}_{0,j}) + b_i(\hat{\boldsymbol{v}}_{0,i} - \boldsymbol{v}_0)$ are the first order and second order estimation error, respectively. The parameters ι_1, ι_2, ι_3, ι_4, η_1 and η_2 are all candidate gains for the convergence performance of distributed estimator (14).

Based on the principle of NSBC approach, the task-space behavioral function $\boldsymbol{\rho}_\mathrm{f} : \mathbb{R}^{3n} \to \mathbb{R}^{2n}$ of FDB is formulated as

$$\boldsymbol{\rho}_\mathrm{f} = \left[\boldsymbol{\rho}_{\mathrm{f},1}^\top, \cdots \boldsymbol{\rho}_{\mathrm{f},n}^\top\right]^\top, \boldsymbol{\rho}_{\mathrm{f},i} = \left[\|\boldsymbol{x}_i - \boldsymbol{x}_{\mathrm{fd},i}\|, \varphi_i\right]^\top, \tag{15}$$

where $\boldsymbol{x}_i = \left[\boldsymbol{q}_i(1), \boldsymbol{q}_i(2)\right]^\top$ and $\boldsymbol{x}_{\mathrm{fd},i} = \left[\boldsymbol{q}_{\mathrm{fd},i}(1), \boldsymbol{q}_{\mathrm{fd},i}(2)\right]^\top$ denote the current position and desired position, respectively. Note that and $\boldsymbol{q}_i = \left[x_i, y_i, \varphi_i\right]^\top$ and $\boldsymbol{q}_{\mathrm{fd},i} = \left[x_{\mathrm{fd},i}, y_{\mathrm{fd},i}, \varphi_{\mathrm{fd},i},\right]^\top$ represent current state and the desired formation state of i^{th} OMR,

respectively. In the distributed formation configuration, the desired formation reference $\boldsymbol{q}_{\mathrm{fd},i}$ requires communication or measurements from neighboring OMRs and the virtual leader. Thereby, it can be designed as

$$\boldsymbol{q}_{\mathrm{fd},i} = \gamma_{\mathrm{fd}}\bigg(\kappa_2(\hat{\boldsymbol{p}}_{0,i} + \boldsymbol{\zeta}_i) + \kappa_2 \sum_{j=1}^{n} a_{ij}(\boldsymbol{p}_j - \boldsymbol{\zeta}_j + \boldsymbol{\zeta}_i)\bigg), \tag{16}$$

where $\gamma_{\mathrm{fd}} = \frac{1}{(\kappa_1+\kappa_2\sum_{j=1}^{n} a_{ij})}$, the coefficient $\kappa_1 \in [0,1]$ is used to tune the weight of formation tracking, and $\kappa_2 \in [0,1]$ governs coordination performance. They satisfy the relationship $\kappa_1 + \kappa_2 = 1$. The $\boldsymbol{\zeta}_i = \left[\boldsymbol{\varrho}_i^\top, \Xi_i\right]^\top$ and $\boldsymbol{\zeta}_j = \left[\boldsymbol{\varrho}_j^\top, \Xi_j\right]^\top$ are the state offset (position and orientation) between virtual leader and i^{th} and j^{th} follower, respectively.

Note that the FDB behavioral function can be converted to be a fully actuated form $\bar{\boldsymbol{\rho}}_{\mathrm{f},i} : \mathbb{R}^3 \to \mathbb{R}^3$, such that

$$\bar{\boldsymbol{\rho}}_{\mathrm{f},i} = f_{\mathrm{f}}(\boldsymbol{q}_i) = \left[\boldsymbol{\rho}_{\mathrm{f},i}^\top, 0\right]^\top, \tag{17}$$

Then, the differential relationship of (17) is

$$\dot{\bar{\boldsymbol{\rho}}}_{\mathrm{f},i} = \boldsymbol{J}_{\mathrm{f},i}(\boldsymbol{q}_i)\boldsymbol{v}_{\mathrm{f},i}, \tag{18}$$

where $\boldsymbol{J}_{\mathrm{f},i}(\boldsymbol{q}_i) = \frac{\partial \bar{\boldsymbol{\rho}}_{\mathrm{f},i}}{\partial \boldsymbol{q}_i} \in \mathbb{R}^{3\times 3}$ is the Jacobian matrix and $\boldsymbol{v}_{\mathrm{f},i} \in \mathbb{R}^3$ is the stacked vector of the i^{th} OMR. The reference velocity $\boldsymbol{v}_{\mathrm{f},i}$ of FDB can be further calculated as

$$\boldsymbol{v}_{\mathrm{f},i} = \boldsymbol{J}_{\mathrm{f},i}^{\dagger}(\dot{\bar{\boldsymbol{\rho}}}_{\mathrm{f},i} + \boldsymbol{\Lambda}_{\mathrm{f}}(\bar{\boldsymbol{\rho}}_{\mathrm{fd},i} - \bar{\boldsymbol{\rho}}_{\mathrm{f},i})), \tag{19}$$

where $\boldsymbol{J}_{\mathrm{f},i}^{\dagger} = \boldsymbol{J}_{\mathrm{f},i}^{\top}(\boldsymbol{J}_{\mathrm{f},i}\boldsymbol{J}_{\mathrm{f},i}^{\top})^{-1}$ is the pseudo-inverse matrix of $\boldsymbol{J}_{\mathrm{f},i}(\boldsymbol{\rho}_i)$ and $\boldsymbol{\Lambda}_{\mathrm{f}}$ is a gain matrix of positive-definite constant. Let $\bar{\boldsymbol{\rho}}_{\mathrm{f},i}, \bar{\boldsymbol{\rho}}_i$ be the desired and actual task function of FDB, respectively. And $\tilde{\boldsymbol{\rho}}_i = \bar{\boldsymbol{\rho}}_{\mathrm{fd},i} - \bar{\boldsymbol{\rho}}_{\mathrm{f},i}$ denotes the task error.

Remark 1. Through variable substitution and augmentation, the behavior control of over-actuated properties is transformed into a generalize fully actuated form, referred to as the fully actuated behavior control strategy. However, the Jacobian matrix resulting from the fully actuated transformation does not always guarantee non-singular. To this end, a pseudo-inverse computation method is employed in this study.

3.1.2. ***Fully Actuated Robot Collision Avoidance Behavior***

This part focuses on the robot collision avoidance behavior, which ensures that a robot avoid collisions with other robots during task execution. As shown in Fig. 3 (a), Robot 1, with a radius-based volume of r, detects the state information of nearby Robot 2 using sensors, and then calculates collision avoidance control signals to ensure their minimum distance remains above the safety threshold R.

Based on the geometric analysis of Fig. 3(a), the task-space behavioral function

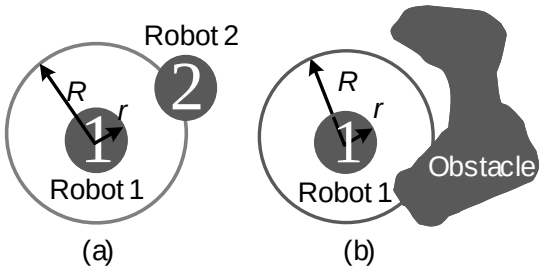

Figure 3. The overall scheme of the fully actuated behavioral control.

$\boldsymbol{\rho}_{\mathrm{c}} : \mathbb{R}^{3n} \to \mathbb{R}^{2n}$ of FRCB can be formulated as

$$\begin{cases} \boldsymbol{\rho}_{\mathrm{c}} = \left[\boldsymbol{\rho}_{\mathrm{c},1}^{\top}, \cdots \boldsymbol{\rho}_{\mathrm{c},n}^{\top}\right]^{\top}, \\ \boldsymbol{\rho}_{\mathrm{c},i} = \left[R - R\sin(\dfrac{\|\boldsymbol{x}_i - \boldsymbol{x}_j\| + R - 4r}{4R - 2r}\pi), \varphi_i\right]^{\top}, \end{cases} \tag{20}$$

where $\boldsymbol{x}_j$ denotes the detected position of OMR in the sensor range of i^{th} OMR. R is the safety threshold, r denotes the radius of OMRs.

Then, the task function of FRCB is converted to be a fully actuated form: $\bar{\boldsymbol{\rho}}_{\mathrm{c},i} : \mathbb{R}^3 \to \mathbb{R}^3$, such that

$$\bar{\boldsymbol{\rho}}_{\mathrm{c},i} = f_{\mathrm{c}}(\boldsymbol{q}_i) = \left[\boldsymbol{\rho}_{\mathrm{c},i}^{\top}, 0\right]^{\top}, \tag{21}$$

Similarly, the reference velocity $\boldsymbol{v}_{\mathrm{c},i}$ of FRCB is

$$\boldsymbol{v}_{\mathrm{c},i} = \boldsymbol{J}_{\mathrm{c},i}^{\dagger}(\dot{\bar{\boldsymbol{\rho}}}_{\mathrm{c},i} + \boldsymbol{\Lambda}_{\mathrm{c}}(\bar{\boldsymbol{\rho}}_{\mathrm{cd},i} - \bar{\boldsymbol{\rho}}_{\mathrm{c},i})), \tag{22}$$

where $\boldsymbol{J}_{\mathrm{c},i}(\boldsymbol{q}_i) = \frac{\partial \bar{\boldsymbol{\rho}}_{\mathrm{c},i}}{\partial \boldsymbol{q}_i} \in \mathbb{R}^{3\times 3}$ is the Jacobian matrix and $\boldsymbol{v}_{\mathrm{c},i} \in \mathbb{R}^3$ is the stacked vector of the i^{th} OMR. $\boldsymbol{J}_{\mathrm{c},i}^{\dagger} = \boldsymbol{J}_{\mathrm{c},i}^{\top}(\boldsymbol{J}_{\mathrm{c},i}\boldsymbol{J}_{\mathrm{c},i}^{\top})^{-1}$ is the pseudo-inverse matrix of $\boldsymbol{J}_{\mathrm{c},i}(\boldsymbol{\rho}_i)$, and $\boldsymbol{\Lambda}_{\mathrm{c}}$ is a gain matrix of positive-definite constant. Let $\bar{\boldsymbol{\rho}}_{\mathrm{c},i}, \bar{\boldsymbol{\rho}}_i$ be the desired and actual task function, respectively. As well as $\tilde{\boldsymbol{\rho}}_i = \bar{\boldsymbol{\rho}}_{\mathrm{cd},i} - \bar{\boldsymbol{\rho}}_{\mathrm{c},i}$ denotes the task error.

3.1.3. ***Fully Actuated Obstacle Collision Avoidance Behavior***

This part focuses on the robot collision avoidance behavior, which ensures that a robot avoid collisions with other detected obstacles during task execution. As shown in Fig. 3 (b), Robot 1, with a radius-based volume of r, detects the state information of nearby detected obstacles using sensors, and then calculates collision avoidance control signals to ensure their minimum distance remains above the safety threshold R.

Based on the geometric analysis of Fig. 3(b), the task-space behavioral function $\boldsymbol{\rho}_{\mathrm{a}} : \mathbb{R}^{3n} \to \mathbb{R}^{2n}$ of FOCB can be formulated as

$$\begin{cases} \boldsymbol{\rho}_{\mathrm{a}} = \left[\boldsymbol{\rho}_{\mathrm{a},1}^{\top}, \cdots \boldsymbol{\rho}_{\mathrm{a},n}^{\top}\right]^{\top}, \\ \boldsymbol{\rho}_{\mathrm{a},i} = \left[R - R\sin(\dfrac{\|\boldsymbol{x}_i - \boldsymbol{x}_{\mathrm{o}}\| + R - 2r}{2R - 2r}\pi), \varphi_i\right]^{\top}, \end{cases} \tag{23}$$

where $\boldsymbol{x}_j$ denotes the detected position of obstacle in the sensor range of i^{th} OMR. R is the safety threshold, r denotes radius of OMR. Then, the task function of FOCB is converted to be a fully actuated form: $\bar{\boldsymbol{\rho}}_{\mathrm{a},i} : \mathbb{R}^3 \to \mathbb{R}^3$, such that

$$\bar{\boldsymbol{\rho}}_{\mathrm{a},i} = f_{\mathrm{a}}(\boldsymbol{q}_i) = \left[\boldsymbol{\rho}_{\mathrm{a},i}^{\top}, 0\right]^{\top}, \tag{24}$$

Similarly, the reference velocity $\boldsymbol{v}_{\mathrm{a},i}$ of FRCB is

$$\boldsymbol{v}_{\mathrm{a},i} = \boldsymbol{J}_{\mathrm{a},i}^{\dagger}(\dot{\bar{\boldsymbol{\rho}}}_{\mathrm{a},i} + \boldsymbol{\Lambda}_{\mathrm{a}}(\bar{\boldsymbol{\rho}}_{\mathrm{ad},i} - \bar{\boldsymbol{\rho}}_{\mathrm{a},i})), \tag{25}$$

where $\boldsymbol{J}_{\mathrm{a},i}(\boldsymbol{q}_i) = \frac{\partial \bar{\boldsymbol{\rho}}_{\mathrm{a},i}}{\partial \boldsymbol{q}_i} \in \mathbb{R}^{3\times 3}$ is the Jacobian matrix and $\boldsymbol{v}_{\mathrm{a},i} \in \mathbb{R}^3$ is the stacked vector of the i^{th} OMR. $\boldsymbol{J}_{\mathrm{a},i}^{\dagger} = \boldsymbol{J}_{\mathrm{a},i}^{\top}(\boldsymbol{J}_{\mathrm{a},i}\boldsymbol{J}_{\mathrm{a},i}^{\top})^{-1}$ is the pseudo-inverse matrix of $\boldsymbol{J}_{\mathrm{a},i}(\boldsymbol{\rho}_i)$, and $\boldsymbol{\Lambda}_{\mathrm{a}}$ is a gain matrix of positive-definite constant. Let $\bar{\boldsymbol{\rho}}_{\mathrm{a},i}, \bar{\boldsymbol{\rho}}_i$ be the desired and actual task function, respectively. As well as $\tilde{\boldsymbol{\rho}}_i = \bar{\boldsymbol{\rho}}_{\mathrm{ad},i} - \bar{\boldsymbol{\rho}}_{\mathrm{a},i}$ denotes the task error.

3.2. Prioritized Multi-behavior Fusion

The prioritized multi-behavior fusion process facilitates the acquisition of the kinematic reference signal. By applying the geometric principles of null-space projection, the velocity outputs of individual elementary behaviors (FDB, FRCB and FOCB) can be effectively combined. These behaviors are subsequently labeled as 1, 2, and 3, respectively. Then, a specific vector $\vartheta \in \mathbb{R}^{3\times 1}$ is used to represent the priority order, with its subscripts indicating the magnitude of priority. Accordingly, this vector is defined as $\vartheta = [3, 1, 2]^{\top}$ when the priority of behaviors satisfies the condition $FOCB > FRCB > FDB$ at a given moment t. As a result, the desired velocity output $\boldsymbol{v}_{\mathrm{d,i}}$ for the i^{th} OMR at time t can be expressed as:

$$\begin{aligned}\boldsymbol{v}_d(t) =& \boldsymbol{v}_{\vartheta(1)} + (\boldsymbol{I}_{\vartheta(1)} - \boldsymbol{J}_{\vartheta(1)}^{\dagger}\boldsymbol{J}_{\vartheta(1)})\big[\boldsymbol{v}_{\vartheta(2)} + (\boldsymbol{I}_{\vartheta(2)} - \boldsymbol{J}_{\vartheta(2)}^{\dagger}\boldsymbol{J}_{\vartheta(2)})\boldsymbol{v}_{\vartheta(3)}\big],\end{aligned} \tag{26}$$

where $\boldsymbol{v}_{\vartheta(1)}$, $\boldsymbol{v}_{\vartheta(2)}$, and $\boldsymbol{v}_{\vartheta(3)}$ represent the kinematic outputs of the elementary behaviors after priority sorting. Similarly, $\boldsymbol{J}_{\vartheta(1)}$, $\boldsymbol{J}_{\vartheta(2)}$, and $\boldsymbol{J}_{\vartheta(3)}$ denote the corresponding Jacobian matrices after priority sorting, while $\boldsymbol{I}_{\vartheta(1)}$, $\boldsymbol{I}_{\vartheta(2)}$, and $\boldsymbol{I}_{\vartheta(3)}$ are identity matrices associated with the dimensions of the respective behavior functions.

The asymptotic stability of the proposed behaviors can be readily proven. However, ensuring the asymptotic stability of the prioritized multi-behavior fusion process is equally crucial. To this end, the corresponding theorem is presented below.

Theorem 3.1. *Consider the cooperative task function $\boldsymbol{\rho}_i = [\boldsymbol{\rho}_{1,i}, \boldsymbol{\rho}_{2,i}, \boldsymbol{\rho}_{3,i}]^{\top}$ which is composed of three elementary behaviors arranged in a priority order $\boldsymbol{\rho}_{1,i} > \boldsymbol{\rho}_{2,i} > \boldsymbol{\rho}_{3,i}$. The task error system $\boldsymbol{e}_i = \boldsymbol{\rho}_i - \boldsymbol{\rho}_{\mathrm{d,i}}$ for the Multi-OMRs achieves large-scale asymptotic stability under any priority conditions when employing the proposed distributed behaviors* (15), (20), (23) *and the prioritized multi-behavior fusion process* (26).

Proof. Consider the following candidate Lyapunov function

$$V_{\rho} = \frac{1}{2}\sum_{i=1}^{n} \boldsymbol{e}_i^{\top}\boldsymbol{\Gamma}_{\rho}\boldsymbol{e}_i, \tag{27}$$

where $\boldsymbol{e}_i = [\boldsymbol{e}_{1,i}, \boldsymbol{e}_{2,i}, \boldsymbol{e}_{3,i}]$, and $\boldsymbol{\Gamma}_\rho = \mathrm{diag}([\gamma_1, \gamma_2, \gamma_3])$ is the positive parameter matrix.

Firstly, taking the time derivative of V_ρ, one can obtain that

$$\begin{aligned}\dot{V}_\rho &= \sum_{i=1}^{n}\left(\gamma_1 \boldsymbol{e}_{1,i}^\top \dot{\boldsymbol{e}}_{1,i} + \gamma_2 \boldsymbol{e}_{2,i}^\top \dot{\boldsymbol{e}}_{2,i} + \gamma_3 \boldsymbol{e}_{3,i}^\top \dot{\boldsymbol{e}}_{3,i}\right)^\top \\ &= -\sum_{i=1}^{n}\left\{\boldsymbol{e}_i^\top \left[\boldsymbol{J}_1, \boldsymbol{J}_2, \boldsymbol{J}_3\right]^\top \left[\gamma_1 \boldsymbol{J}_1^\dagger \boldsymbol{\Lambda}_1 \boldsymbol{e}_{1,i}, \gamma_2 \boldsymbol{N}_1 \boldsymbol{J}_2^\dagger \boldsymbol{\Lambda}_2 \boldsymbol{e}_{2,i}, \gamma_3 \boldsymbol{N}_{1,2} \boldsymbol{J}_3^\dagger \boldsymbol{\Lambda}_3 \boldsymbol{e}_{3,i}\right]\right\} \\ &= -\sum_{i=1}^{n}(\boldsymbol{e}_i^\top \boldsymbol{Q} \boldsymbol{e}_i),\end{aligned} \tag{28}$$

where $\boldsymbol{N}_1 = \boldsymbol{I} - \boldsymbol{J}_1^\dagger \boldsymbol{J}_1, \boldsymbol{N}_2 = \boldsymbol{I} - \boldsymbol{J}_2^\dagger \boldsymbol{J}_2$ are the null-space projection operators corresponding to the highest-priority and second-priority behaviors, respectively. $\boldsymbol{N}_{1,2} = \boldsymbol{N}_1 \boldsymbol{N}_2$. The matrix $\boldsymbol{Q} = [Q_{ab}] \in \mathbb{R}^{3\times 3}(a, b = 1, 2, 3)$ can be defined as

$$\boldsymbol{Q} = \begin{bmatrix} \gamma_1 \boldsymbol{\Lambda}_1 & \gamma_2 \boldsymbol{J_1} \boldsymbol{N_1} \boldsymbol{J_2^\dagger} \boldsymbol{\Lambda}_2 & \gamma_3 \boldsymbol{J_1} \boldsymbol{N_{1,2}} \boldsymbol{J_3^\dagger} \boldsymbol{\Lambda}_3 \\ \gamma_1 \boldsymbol{J_2} \boldsymbol{J_1^\dagger} \boldsymbol{\Lambda}_1 & \gamma_2 \boldsymbol{J_2} \boldsymbol{N_1} \boldsymbol{J_2^\dagger} \boldsymbol{\Lambda}_2 & \gamma_3 \boldsymbol{J_2} \boldsymbol{N_{1,2}} \boldsymbol{J_3^\dagger} \boldsymbol{\Lambda}_3 \\ \gamma_1 \boldsymbol{J_3} \boldsymbol{J_1^\dagger} \boldsymbol{\Lambda}_1 & \gamma_2 \boldsymbol{J_3} \boldsymbol{N_1} \boldsymbol{J_2^\dagger} \boldsymbol{\Lambda}_2 & \gamma_3 \boldsymbol{J_3} \boldsymbol{N_{1,2}} \boldsymbol{J_3^\dagger} \boldsymbol{\Lambda}_3 \end{bmatrix}. \tag{29}$$

To ensure the stability of the Multi-OMRs (6), the matrix $\boldsymbol{Q}$ in (28) must be positive definite. Then, defined the $\overline{\lambda}(\boldsymbol{A}_s)$ and $\underline{\lambda}(\boldsymbol{A}_s)$ are the maximum and minimum singular values of matrix $\boldsymbol{A}_s$, respectively. Note that the expressions $\|\boldsymbol{J}_1\| = \|\boldsymbol{J}_2\| = \|\boldsymbol{J}_3\| = 1$, $\|\boldsymbol{N}_1\| \leqslant 1, \|\boldsymbol{N}_2\| \leqslant 1$, and $\|\boldsymbol{N}_3\| \leqslant 1$, $\boldsymbol{J}_1\boldsymbol{N}_1 = 0, \boldsymbol{J}_2\boldsymbol{N}_2 = 0$. By using property of $\overline{\lambda}(\boldsymbol{A}_s\boldsymbol{B}_s) \leqslant \overline{\lambda}(\boldsymbol{A}_s)\overline{\lambda}(\boldsymbol{B}_s)$ and $\underline{\lambda}(\boldsymbol{A}_s\boldsymbol{B}_s) > \underline{\lambda}(\boldsymbol{A}_s)\underline{\lambda}(\boldsymbol{B}_s)$, the equation (28) is derived as

$$\begin{aligned}\dot{V}_\rho \leqslant -\sum_{i=1}^{n}\Big[&\underline{\lambda}(\boldsymbol{Q}_{11})\|\boldsymbol{e}_{1,i}\|^2 + \underline{\lambda}(\boldsymbol{Q}_{22})\|\boldsymbol{e}_{2,i}\|^2 + \underline{\lambda}(\boldsymbol{Q}_{33})\|\boldsymbol{e}_{3,i}\|^2 - \overline{\lambda}(\boldsymbol{Q}_{21})\|\boldsymbol{e}_{2,i}\|\|\boldsymbol{e}_{1,i}\| \\ &- \overline{\lambda}(\boldsymbol{Q}_{31})\|\boldsymbol{e}_{3,i}\|\|\boldsymbol{e}_{1,i}\| - 2\max(\overline{\lambda}(\boldsymbol{Q}_{32}), \overline{\lambda}(\boldsymbol{Q}_{23}))\|\boldsymbol{e}_{3,i}\|\|\boldsymbol{e}_{2,i}\|\Big] \leqslant -\sum_{i=1}^{n}(\hat{\boldsymbol{e}}_i^\top \hat{\boldsymbol{Q}} \hat{\boldsymbol{e}}_i),\end{aligned} \tag{30}$$

where the modified norm vector is defined as $\hat{\boldsymbol{e}}_i = \left[\|\boldsymbol{e}_{1,i}^\top\|, \|\boldsymbol{e}_{2,i}^\top\|, \|\boldsymbol{e}_{3,i}^\top\|\right]^\top$, and the modified coefficient matrix $\hat{\boldsymbol{Q}} = [\hat{Q}_{ab}] \in \mathbb{R}^{3\times 3}(a, b = 1, 2, 3)$ represents a symmetric matrix. The elements of this matrix are listed as follows:

$$\begin{cases} \hat{Q}_{11} = \gamma_1 \underline{\lambda}(\boldsymbol{Q}_{11}\boldsymbol{\Lambda}_1^{-1})\underline{\lambda}(\boldsymbol{\Lambda}_1), \\ \hat{Q}_{22} = \gamma_2 \underline{\lambda}(\boldsymbol{Q}_{22}\boldsymbol{\Lambda}_2^{-1})\underline{\lambda}(\boldsymbol{\Lambda}_2), \\ \hat{Q}_{33} = \gamma_3 \underline{\lambda}(\boldsymbol{Q}_{33}\boldsymbol{\Lambda}_3^{-1})\underline{\lambda}(\boldsymbol{\Lambda}_3), \\ \hat{Q}_{12} = \hat{Q}_{21} = -\dfrac{1}{2}\gamma_2 \overline{\lambda}(\boldsymbol{Q}_{21}\boldsymbol{\Lambda}_1^{-1})\overline{\lambda}(\boldsymbol{\Lambda}_1), \\ \hat{Q}_{13} = \hat{Q}_{31} = -\dfrac{1}{2}\gamma_3 \overline{\lambda}(\boldsymbol{Q}_{31}\boldsymbol{\Lambda}_2^{-1})\overline{\lambda}(\boldsymbol{\Lambda}_1), \\ \hat{Q}_{23} = \hat{Q}_{32} = -\gamma_2 \max\left[\overline{\lambda}(\boldsymbol{Q}_{32}), \overline{\lambda}(\boldsymbol{Q}_{23})\right]. \end{cases} \tag{31}$$

To ensure the stability of the Multi-OMRs in (6), the matrix $\hat{\boldsymbol{Q}}$ must similarly

be positive definite. This requires that all the determinants of its principal minors are greater than zero. The stable conditions of the cooperative task function can be expressed as

$$\begin{cases} \underline{\lambda}(\boldsymbol{\Lambda}_1) > 0, \quad \underline{\lambda}(\boldsymbol{\Lambda}_2) > \max\left\{0, \dfrac{\gamma_2\left[\overline{\lambda}(\boldsymbol{J_2 N_1 J_1^\dagger})\right]^2 \underline{\lambda}(\boldsymbol{\Lambda}_1)}{4\gamma_1 \overline{\lambda}(\boldsymbol{J_2 N_1 J_2^\dagger})}\right\}, \quad \underline{\lambda}(\boldsymbol{\Lambda}_3) > \\ \max\left\{0, \dfrac{\gamma_2\left[\max\left(\overline{\lambda}(\boldsymbol{Q}_{32}), \overline{\lambda}(\boldsymbol{Q}_{23})\right)\right]^2}{\gamma_3 \overline{\lambda}(\boldsymbol{J_2 N_1 J_2^\dagger})\overline{\lambda}(\boldsymbol{J_3 N_{1,2} J_3^\dagger})\underline{\lambda}(\boldsymbol{\Lambda}_2)}, \dfrac{-2\max\left(\overline{\lambda}(\boldsymbol{Q}_{32}), \overline{\lambda}(\boldsymbol{Q}_{23})\right)\overline{\lambda}(\boldsymbol{J_3 J_1^\dagger})}{\overline{\lambda}(\boldsymbol{J_3 N_{1,2} J_3^\dagger})\underline{\lambda}(\boldsymbol{\Lambda}_2)}\right\}. \end{cases} \tag{32}$$

Based on the derived conditions (32), one can obtain

$$\dot{V}_\rho \leqslant -\sum_{i=1}^{n}(\hat{\boldsymbol{e}}_i^\top \underline{\lambda}(\hat{\boldsymbol{Q}})\hat{\boldsymbol{e}}_i) \leqslant 0 \tag{33}$$

where $\underline{\lambda}(\hat{\boldsymbol{Q}})$ is the minimum singular value of $\hat{\boldsymbol{Q}}$.

Therefore, The task error system $\boldsymbol{e}_i = \boldsymbol{\rho}_i - \boldsymbol{\rho}_{\mathrm{d,i}}$ will converge to a neighborhood around zero under any priority conditions when employing the proposed distributed behaviors (15), (20), (23), and the prioritized multi-behavior fusion process (26). □

However, achieving the asymptotic convergence-guaranteed formation control for the closed-loop Multi-OMRs still necessitates a behavioral tracking controller capable of handling system nonlinearities and model uncertainty.

3.3. Fully Actuated Behavioral Controller Design

In this section, under *Assumption 2.1* a sliding mode behavioral tracking controller is designed for the Multi-OMRs. From the error system (6) of the Multi-OMRs, it can be observed that the system input coefficient matrix $\boldsymbol{B}_i \in \mathbb{R}^{3\times 4}$ is not a square matrix but rather exhibits an over-actuated property. Fortunately, an over-actuated system can be transformed into a fully actuated system using the variable augmentation method (Duan, 2024). Therefore, the error system (6) can be transformed into a fully actuated system to facilitate controller design.

3.3.1. Fully Actuated Conversion

The following transformation operations are implemented:

$$\begin{aligned} &\bar{\boldsymbol{q}}_{\mathrm{d},i} = \begin{bmatrix} \boldsymbol{q}_{\mathrm{d},i} \\ \boldsymbol{O}_{1\times 1} \end{bmatrix}, \bar{\boldsymbol{e}}_i = \begin{bmatrix} \boldsymbol{e}_i \\ \boldsymbol{O}_{1\times 1} \end{bmatrix}, \bar{\boldsymbol{d}}_i = \begin{bmatrix} \boldsymbol{d}_i \\ \boldsymbol{O}_{1\times 1} \end{bmatrix}, \\ &\bar{\boldsymbol{A}}_{0,i} = \begin{bmatrix} \boldsymbol{A}_{0,i} & \boldsymbol{O}_{1\times 1} \\ \boldsymbol{O}_{1\times 3} & \boldsymbol{O}_{1\times 1} \end{bmatrix}, \bar{\boldsymbol{A}}_{1,i} = \begin{bmatrix} \boldsymbol{A}_{1,i} \\ \boldsymbol{O}_{1\times 1} \end{bmatrix}, \bar{\boldsymbol{B}}_i = \begin{bmatrix} \boldsymbol{B}_i \\ \boldsymbol{O}_{1\times 4} \end{bmatrix}, \end{aligned} \tag{34}$$

where $\boldsymbol{O}_{a\times b}$ denotes a zero matrix of dimension $a \times b$, then the system (6) is converted into the fully actuated form:

$$\ddot{\bar{\boldsymbol{e}}}_i + \ddot{\bar{\boldsymbol{q}}}_{\mathrm{d},i} + \bar{\boldsymbol{A}}_{1,i} + \bar{\boldsymbol{A}}_{0,i}\dot{\bar{\boldsymbol{e}}}_i + \bar{\boldsymbol{A}}_{0,i}\dot{\bar{\boldsymbol{q}}}_{\mathrm{d},i} - \bar{\boldsymbol{d}}_i = \bar{\boldsymbol{B}}_i \boldsymbol{u}_i. \tag{35}$$

Note that the system input coefficient matrix $\bar{\boldsymbol{B}}_i \in \mathbb{R}^{4\times4}$ here is non-singular, $\det(\boldsymbol{B}_i) \neq 0$) in designed Multi-OMRs.

3.3.2. ***Fully Actuated Control Law***

To enable the robots in Multi-OMRs to track their composite task-space behaviors, the *Definition 2.3* and *Lemma 2.4* indicate that the fully actuated system (35) for Multi-OMRs can be stabilized using the following controller

$$\boldsymbol{u}_i = -\bar{\boldsymbol{B}}_i^{-1}(-\bar{\boldsymbol{A}}_{0,i}\dot{\bar{\boldsymbol{e}}}_i - \bar{\boldsymbol{A}}_{1,i} - \ddot{\bar{\boldsymbol{q}}}_{\mathrm{d},i} - \bar{\boldsymbol{A}}_{0,i}\dot{\bar{\boldsymbol{q}}}_{\mathrm{d},i} + \boldsymbol{\Gamma}_i), \tag{36}$$

where $\boldsymbol{\Gamma}_i$ denotes the control term to be designed. Then, by substituting the expression of the controller (36) into system (35), the error system equation (36) is rewritten as

$$\ddot{\bar{\boldsymbol{e}}}_i = \boldsymbol{\Gamma}_i + \boldsymbol{D}_i, \tag{37}$$

where $\boldsymbol{D}_i$ denotes the total uncertainty of i^{th} OMR. However, the instantaneous magnitude of the model uncertainty of OMR is typically unknown in advance. To this end, an extended state observer (ESO) is designed to provide the real-time observation of the total uncertainty $\boldsymbol{D}_i$.

3.3.3. ***ESO Design***

Then, the total model uncertainty $\boldsymbol{D}_i$ is expanded into a new state variable $\boldsymbol{z}_{2,i}$ for the fully actuated system (35), such that $\boldsymbol{z}_{2,i} = \boldsymbol{D}_i$. And define $\boldsymbol{z}_{1,i} = \dot{\bar{\boldsymbol{e}}}_i$. With these definitions, the fully actuated system (35) can be rewritten as:

$$\begin{cases} \boldsymbol{z}_{1,i} = \boldsymbol{\Gamma}_i + \boldsymbol{z}_{2,i}, \\ \boldsymbol{z}_{2,i} = \boldsymbol{\varepsilon}_i, \\ \boldsymbol{Y}_i \ \ = \boldsymbol{z}_{1,i}, \end{cases} \tag{38}$$

where $\boldsymbol{\varepsilon}_i = \dot{\boldsymbol{D}} = [\varepsilon_{1,i}, \varepsilon_{2,i}, \varepsilon_{3,i}]^\top$ represents the first derivative of the total uncertainty, and $\boldsymbol{Y}_i$ denotes the output of the fully actuated system in (35). To ensure that the uncertainty are estimable and compensable, the following necessary assumption is proposed:

Assumption 3.2. *The first derivative of total uncertainty $\boldsymbol{\varepsilon}_i = [\varepsilon_{1,i}, \varepsilon_{2,i}, \varepsilon_{3,i}]^\top$ is bounded, for $\forall t \in [0, \infty)$, the elements $\boldsymbol{\varepsilon}_{k,i}, k = 1, 2, 3$, satisfy the following inequality $|\boldsymbol{\varepsilon}_{k,i}| \leqslant \bar{\boldsymbol{\varepsilon}}$, where $\bar{\boldsymbol{\varepsilon}} \in (0, \infty)$ is a unknown positive constant.*

Then, denote $\widehat{\boldsymbol{z}}_{1,i}, \widehat{\boldsymbol{z}}_{2,i}$ as the output of the ESO in i^{th} OMR. Defined $\boldsymbol{\epsilon}_{1,i} = \boldsymbol{z}_{1,i} - \widehat{\boldsymbol{z}}_{1,i}$, and $\boldsymbol{\epsilon}_{2,i} = \boldsymbol{z}_{2,i} - \widehat{\boldsymbol{z}}_{2,i}$ as the estimation errors in equation (38). Therefore, the ESO for the fully actuated system (35) can be designed as

$$\begin{cases} \dot{\widehat{\boldsymbol{z}}}_{1,i} = \boldsymbol{\Gamma}_i + \widehat{\boldsymbol{z}}_{2,i} + \mu_1 \mathrm{sig}^{r_1}(\boldsymbol{\epsilon}_{1,i}), \\ \dot{\widehat{\boldsymbol{z}}}_{2,i} = \mu_2 \mathrm{sig}^{r_2}(\boldsymbol{\epsilon}_{1,i}), \end{cases} \tag{39}$$

where $\mu_1, \mu_2 \in (0, \infty)$, $r_1 \in (0.5, 1)$ and $r_2 = 2r_1 - 1$ are the ESO parameters. The output $\boldsymbol{z}_{2,i}$ generated by the ESO in (39) is capable of driving the estimation errors $\boldsymbol{\epsilon}_{1,i}$ and $\boldsymbol{\epsilon}_{2,i}$ toward a neighborhood of zero within a finite time. The relevant proof

of convergence is presented in (Sun, Wu, & Zhang, 2023). Consequently, real-time estimation of the total uncertainty $\boldsymbol{D}_i$ is achieved.

3.3.4. ***Predefined-time Sliding Mode Control Term Design***

Firstly, based on the sliding mode control technology, the sliding surface for error system (35) is designed as

$$\boldsymbol{s}_i = \dot{\bar{\boldsymbol{e}}}_i + \psi(\bar{\boldsymbol{e}}_i). \tag{40}$$

The term of $\psi(\boldsymbol{e}_i)$ is designed as

$$\psi(\bar{\boldsymbol{e}}_i) = \frac{2}{\alpha_{\mathrm{p}}\mu_{\mathrm{p}}T_{\mathrm{p}}}\left(\|\bar{\boldsymbol{e}}_i\|^{-\alpha_{\mathrm{p}}} + \mu_{\mathrm{p}}^2\|\bar{\boldsymbol{e}}_i\|^{\alpha_{\mathrm{p}}}\right)\bar{\boldsymbol{e}}_i, \tag{41}$$

where $\gamma > 0$ is a given parameter. Under the classical Lyapunov theory, the controller term $\boldsymbol{\Gamma}_i$ in $\boldsymbol{u}_i$ can be designed as

$$\boldsymbol{\Gamma}_i = -\frac{2}{\alpha_{\mathrm{p}}\mu_{\mathrm{p}}T_{\mathrm{p}}}\left(\left(\frac{1}{2}\right)^{\frac{2-\alpha_{\mathrm{p}}}{2}}\|\boldsymbol{s}_i\|^{-\alpha_{\mathrm{p}}} + \left(\frac{1}{2}\right)^{\frac{2+\alpha_{\mathrm{p}}}{2}}\mu_{\mathrm{p}}^2\|\boldsymbol{s}_i\|^{\alpha_{\mathrm{p}}}\right)\boldsymbol{s}_i - \widehat{\boldsymbol{z}}_{2,i} - \dot{\psi}(\bar{\boldsymbol{e}}_i) - \frac{1}{2\upsilon^2}\boldsymbol{s}_i, \tag{42}$$

where υ is a parameter determined by the stability. In summary, the following theorem for this controller is proposed.

Theorem 3.3. *The Multi-OMRs in the proposed fully actuated behavioral tracking control scheme can be stable when executing the proposed ESO* (39) *and controller* (36),(42). *All states in the error system* (35) *will converge to a small region of* $\Omega = \left\{\bar{\boldsymbol{e}}_i \in \mathbb{R}^n \mid V_{\mathrm{p}}(\bar{\boldsymbol{e}}_i) \leqslant \min\left\{a_1, a_2\right\}\right\}$, *where* $a_1 = (2\eta\alpha_{\mathrm{p}}\mu_{\mathrm{p}}T_{\mathrm{p}})^{\frac{2}{2-\alpha_{\mathrm{p}}}}, a_2 = (2\eta\alpha_{\mathrm{p}}\mu_{\mathrm{p}}^2T_{\mathrm{p}})^{\frac{2}{2+\alpha_{\mathrm{p}}}}$, *within a predefined time* $\sqrt{2}T_{\mathrm{p}}$.

Proof. The candidate Lyapunov function can be chosen as

$$V_{\mathrm{p}} = \frac{1}{2}\sum_{i=1}^{n}\boldsymbol{s}_i^{\top}\boldsymbol{s}_i. \tag{43}$$

Then, taking the time derivative of V_{p}, one can obtain

$$\dot{V}_{\mathrm{p}} = \sum_{i=1}^{n}\left(\boldsymbol{s}_i^{\top}\left(\boldsymbol{\Gamma}_i + \boldsymbol{D}_i + \dot{\psi}(\bar{\boldsymbol{e}}_i)\right)\right). \tag{44}$$

Further, by substituting the controller (36) and (42) into (44), one can obtain

$$\begin{aligned}\dot{V}_{\mathrm{p}} &= \sum_{i=1}^{n}\left\{-\gamma_{\mathrm{p}}\boldsymbol{s}_i^{\top}\left[\left(\frac{1}{2}\right)^{\frac{2-\alpha_{\mathrm{p}}}{2}}\|\boldsymbol{s}_i\|^{-\alpha_{\mathrm{p}}} + \left(\frac{1}{2}\right)^{\frac{2+\alpha_{\mathrm{p}}}{2}}\mu_{\mathrm{p}}^2\|\boldsymbol{s}_i\|^{\alpha_{\mathrm{p}}}\right]\boldsymbol{s}_i + \boldsymbol{s}_i^{\top}\boldsymbol{\epsilon}_{2,i} - \frac{1}{2\upsilon^2}\boldsymbol{s}_i^{\top}\boldsymbol{s}_i\right\} \\ &\leqslant \sum_{i=1}^{n}\left\{-\gamma_{\mathrm{p}}\left[\left(\frac{1}{2}\|\boldsymbol{s}_i\|^2\right)^{\frac{2-\alpha_{\mathrm{p}}}{2}} + \mu_{\mathrm{p}}^2\left(\frac{1}{2}\|\boldsymbol{s}_i\|^2\right)^{\frac{2+\alpha_{\mathrm{p}}}{2}}\right]\boldsymbol{s}_i + \boldsymbol{s}_i^{\top}\boldsymbol{\epsilon}_{2,i} - \frac{1}{2\upsilon^2}\boldsymbol{s}_i^{\top}\boldsymbol{s}_i\right\}.\end{aligned} \tag{45}$$

where $\gamma_{\mathrm{p}} = \frac{2}{\alpha_{\mathrm{p}}\mu_{\mathrm{p}}T_{\mathrm{p}}}$. Using *Mean value theorem*, one can obtain that

$$\boldsymbol{s}_i^{\top}\boldsymbol{\epsilon}_{2,i} \leqslant \frac{1}{2\upsilon^2}\boldsymbol{s}_i^{\top}\boldsymbol{s}_i + \frac{\upsilon^2}{2}\boldsymbol{\epsilon}_{2,i}^{\top}\boldsymbol{\epsilon}_{2,i}, \tag{46}$$

where $0 < \upsilon < 2$ is a weight coefficient.

Note that the estimation errors of the ESO (39) are bounded when *Assumption 3.2* holds. This means that for all $\forall t \in [0, \infty)$, there exists a positive constant ϱ such that the condition $\boldsymbol{\epsilon}_{2,i}^{\top}\boldsymbol{\epsilon}_{2,i} < \varrho$ is satisfied. Next, by substituting inequality (46) into the relation (45), the inequality can be further simplified as

$$\dot{V}_{\mathrm{p}} \leqslant \sum_{i=1}^{n}\Big(-\frac{2}{\alpha_{\mathrm{p}}\mu_{\mathrm{p}}T_{\mathrm{p}}}\big(V_{\mathrm{p}}^{1-\frac{\alpha_{\mathrm{p}}}{2}} + \mu_{\mathrm{p}}^2 V_{\mathrm{p}}^{1+\frac{\alpha_{\mathrm{p}}}{2}}\big) + \eta\Big), \tag{47}$$

where $\eta = \frac{\upsilon^2\varrho}{2}$. This inequality satisfies the criterion of *Lemma 1* in (Sun et al., 2023). Therefore, the fully actuated system (35) is said the practical tunable predefined-time stable, such that all state errors in the Multi-OMRs will converge to a small region of $\Omega = \big\{\bar{\boldsymbol{e}}_i \in \mathbb{R}^n \mid V_{\mathrm{p}}(\bar{\boldsymbol{e}}_i) \leqslant \min\big\{a_1, a_2\big\}\big\}$, where $a_1 = (2\eta\alpha_{\mathrm{p}}\mu_{\mathrm{p}}T_{\mathrm{p}})^{\frac{2}{2-\alpha_{\mathrm{p}}}}, a_2 = (2\eta\alpha_{\mathrm{p}}\mu_{\mathrm{p}}^2T_{\mathrm{p}})^{\frac{2}{2+\alpha_{\mathrm{p}}}}$, within predefined time $\sqrt{2}T_{\mathrm{p}}$. □

Based on the conclusions drawn from the proofs of *Theorem 1* and *Theorem 2*, the proposed fully actuated behavioral control scheme ensures collision-free distributed formation control for Multi-OMRs. Furthermore, it is theoretically proven that the task error system of the Multi-OMRs exhibits large-scale asymptotic stability.

4. Numerical simulation results

In this section, a simulation in two-dimensional space under scenarios with model uncertainty is presented for the proposed fully actuated behavioral control algorithm. In the simulation, three OMRs move according to the preset distributed trajectories. The key parameters used in the simulation, including the gain parameters for the proposed distributed fully actuated behaviors, the configuration of the Multi-OMRs, and the parameters for the fully actuated behavioral controller, are shown in Table 2. Both sets of simulations were conducted using MATLAB 2024a.

The desired trajectory of virtual leader is $\boldsymbol{q}_0 = [-40\cos(t+0.5), 16\sin(2t+1)]^{\top}$, $t \in [0, 24]$, which satisfy the bound requirements in *Assumption 2.2*. Then, the initial positions and velocities of robots in Multi-OMRs are given as $\boldsymbol{q}_1(0) = [4.4, -17.5]^{\top}, \boldsymbol{v}_1(0) = [0, 0]^{\top}, \boldsymbol{q}_2(0) = [16.4, -23.5]^{\top}, \boldsymbol{v}_2(0) = [-1.6, 0.2]^{\top}, \boldsymbol{q}_3(0) = [16.4, -5.5]^{\top}, \boldsymbol{v}_3(0) = [0, 0]^{\top}$. The initial estimating positions and velocity of the distributed estimator are given as $\hat{\boldsymbol{q}}_0(0) = \boldsymbol{p}(0)$ and $\hat{\boldsymbol{v}}_0(0) = \boldsymbol{v}(0)$, respectively. And the initial value of ESO (41) is given as $\widehat{\boldsymbol{z}}_1(0) = \dot{\widehat{\boldsymbol{z}}}_1(0) = \boldsymbol{O}_{4\times 5}$. The environmental obstacles in the workspace of Multi-OMRs are designed as $\boldsymbol{x}_{\mathrm{o},1} = [-35, 0]^{\top}, \boldsymbol{x}_{\mathrm{o},2} = [38, -19]^{\top}, \boldsymbol{x}_{\mathrm{o},3} = [12, -15.2]^{\top}, \boldsymbol{x}_{\mathrm{o},4} = [-1, 8]^{\top}, \boldsymbol{x}_{\mathrm{o},5} = [8, -2]^{\top}$. Finally, the affine image of the nominal configuration is designed as $\boldsymbol{\varrho} = [I_n \otimes \boldsymbol{W}(t)]\,\boldsymbol{r} + \mathbf{1}_n \otimes \boldsymbol{b}(t)$, the affine matrix and the constant configuration of robots are calculated as

$$\boldsymbol{W}(t) = \begin{bmatrix} \cos(\psi(t)) & -\sin(\psi(t)) \\ \sin(\psi(t)) & \cos(\psi(t)) \end{bmatrix}\boldsymbol{S}, \boldsymbol{r} = \begin{bmatrix} 0 & -4 & -4 \\ 0 & -4 & -4 \end{bmatrix}, \boldsymbol{b}(t) = \begin{bmatrix} 0 \\ 0 \end{bmatrix} \tag{48}$$

Table 2. Parameter values in the simulation

Parameters	Value
Wheel radius of OMRs, R	$0.0375m$
Total Multi-OMRs of a OMR, m	$1.2kg$
Moment of inertia about z-axis, I_z	$0.01kg \cdot m^2$
Moment of inertia about wheel axis, I_w	$0.02kg \cdot m^2$
Distance between shafts of OMRs, $2l$	$0.06m$
Distance between wheel of OMRs, $2w$	$0.04m$
Static friction coefficient, C_{f}	0.125
Viscous friction coefficient, C_θ	0.2
Gain matrix of FDB, $\mathbf{\Lambda}_{\mathrm{f}}$	$\mathrm{diag}([12, 0.25])$,
Gain matrix of FOCB, $\mathbf{\Lambda}_{\mathrm{a}}$	$\mathrm{diag}([24, 0.25])$,
Gain matrix of FRCB, $\mathbf{\Lambda}_{\mathrm{c}}$	$\mathrm{diag}([32, 0.25])$,
Distributed estimator parameters, $\iota_1, \iota_2, \iota_3, \iota_4, \eta_1, \eta_2$	$0.1, 0.1, 25, 6, \frac{3}{2}, \frac{3}{2}$
Detecting sensing distance, r_{det}	$8m$
Body radius of robot, r	$0.5m$
Safe distance for obstacle collision avoidance, R_{a}	$2m$
Safe distance for robot collision avoidance, R_{c}	$1.6m$
Controller parameters, $\alpha_{\mathrm{p}}, \mu_{\mathrm{p}}, T_{\mathrm{p}}, \upsilon$	$0.5, 30, 4, 1.5$
ESO parameters, μ_1, μ_2, r_1, r_2	$0.6, 0.2, 0.7, 0.4$

where $\boldsymbol{S} = \mathrm{diag}\left([s_{\mathrm{x}}(t), s_{\mathrm{y}}(t)]\right)$ represents a scale factor matrix, which is set by $\mathrm{diag}([1, 1])$ in normal state,$\mathrm{diag}([1, 0.5])$ in middle passage and $\mathrm{diag}([1, 0])$ in narrow passage. $\psi(t) = \arctan(\frac{\boldsymbol{q}_0(2)}{\boldsymbol{q}_0(1)})$ denotes the orientation angle for the formation. The adjacency matrix, leader adjacency matrix and uncertainty of system are defined as

$$\boldsymbol{\mathcal{A}} = \begin{bmatrix} 1 & 0 & 0 \\ 1 & 0 & 0 \\ 1 & 1 & 0 \end{bmatrix}, \boldsymbol{\mathcal{B}} = \begin{bmatrix} 1 \\ 0 \\ 0 \end{bmatrix}, \boldsymbol{d}_i(t) = \begin{bmatrix} 1 + 2\cos(0.3t) \\ 2 + 1.5\sin(0.3t) + 3\cos(0.3t) \\ 3 + 2\sin(0.2t) \\ 2.5 + \sin(0.1t) \end{bmatrix} 10^{-2}\mathrm{N} \cdot \mathrm{m} \quad (49)$$

Therefore, using our fully actuated behavioral control scheme and given parameters, the simulation results are as follows.

Firstly, as illustrated in Fig. 4, all three OMRs successfully track the desired formation positions and orientation angle signals. The OMRs initially converge from different starting states into the desired formation. Through distributed communication, they subsequently follow the desired trajectory of a virtual leader. During this process, each OMR autonomously makes decisions and executes control actions to avoid obstacles, then re-converges into the desired formation. The car-liked marker snapshots, captured at t=0s, 0.96s, 8.4s, 10.8s, 15s and 24s, vividly demonstrate that the proposed fully actuated behavioral control scheme is effective in both establishing and maintaining the desired formation for the Multi-OMRs.

Then, the behavioral tracking performance of the Multi-OMRs is illustrated in Fig. 5 (a). From the results, it is evident that despite starting from different initial conditions, all OMRs successfully accomplish their distributed formation control tasks. This demonstrates that the fully actuated behavioral control scheme ensures a smooth transient process while guaranteeing fully actuated stability within the task space of

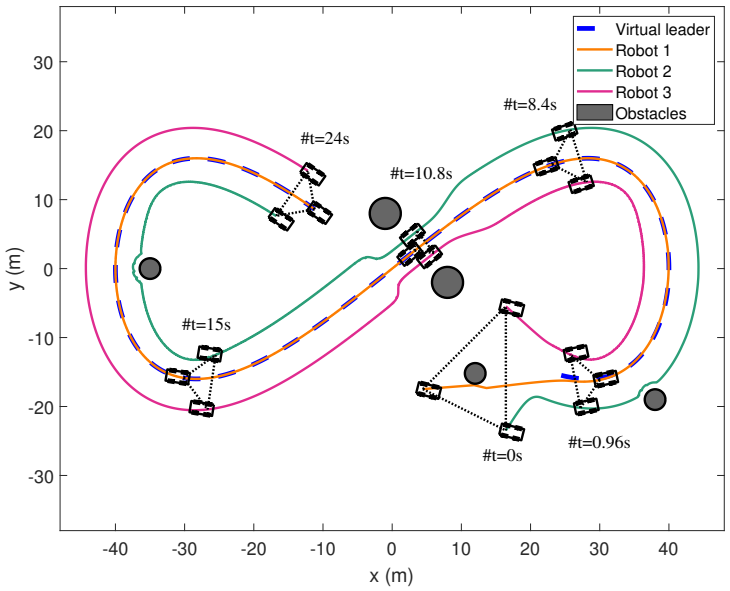

Figure 4. Trajectory of the OMRs: Three robots are executing the formation task through communication via given graph. The snapshots illustrate the states of the robot at times t=0s, 0.96s, 8.4s, 10.8s, 15s and 24s.

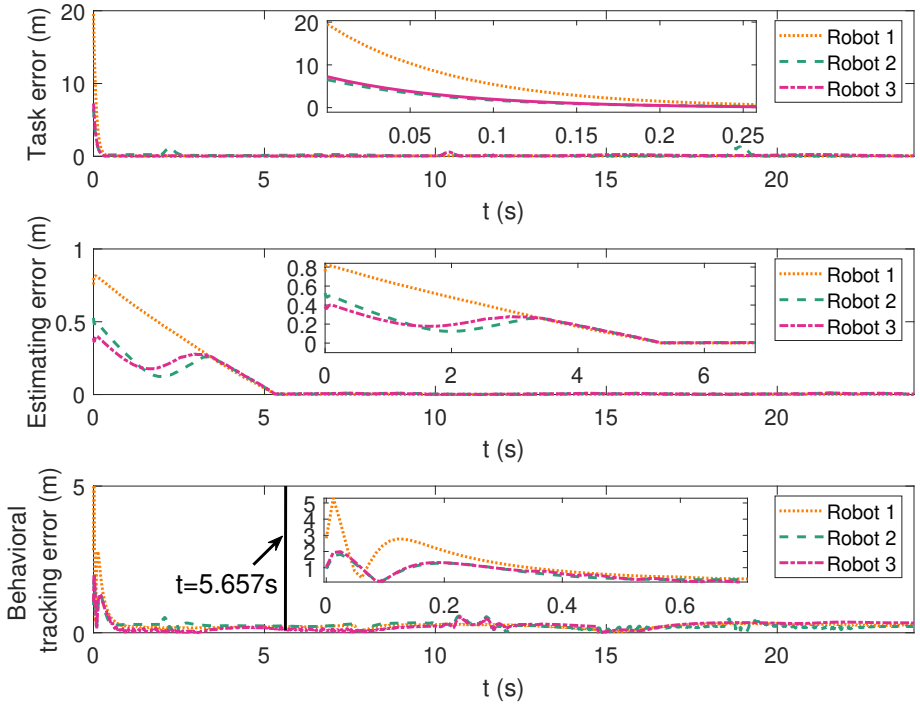

Figure 5. Three error curves: (a) The norm of the behavioral task-space error; (b) The norm of the estimating error of the distributed estimator; (c) The norm of the behavioral tracking error.

the Multi-OMRs. Furthermore, the task error shown in Fig.5(a), the estimation error in Fig.5(b), and the behavioral tracking errors in Fig. 5(c) all converge rapidly and smoothly to values close to zero, which demonstrates the effectiveness of the fully actuated behaviors and tracking controller. The settling time for behavioral tracking errors is observed to be less than the predefined time bound $t = \sqrt{(2)}T_{\mathrm{p}} = 5.657s$. This demonstrated the effectiveness of the fully actuated tracking controller.

Finally, Fig. 6 (a) and (b) present the distances between the OMRs and the obstacles, as well as the distances among the OMRs themselves. Notably, sensor data is sampled and recorded only when the distances fall within the detection range. The proposed FRCB and FOCB effectively regulate all distances, ensuring they remain below the preset safety threshold. This demonstrates the robustness and effectiveness of the fully actuated behavioral control scheme in managing both dynamic and static obstacles, even in complex environments. The control input of the OMRs is shown in Fig. 6(c). The results indicate that the control input remains stable, exhibiting minimal oscillations and no abrupt changes.

Based on the simulation results, the large-scale asymptotic convergence of the

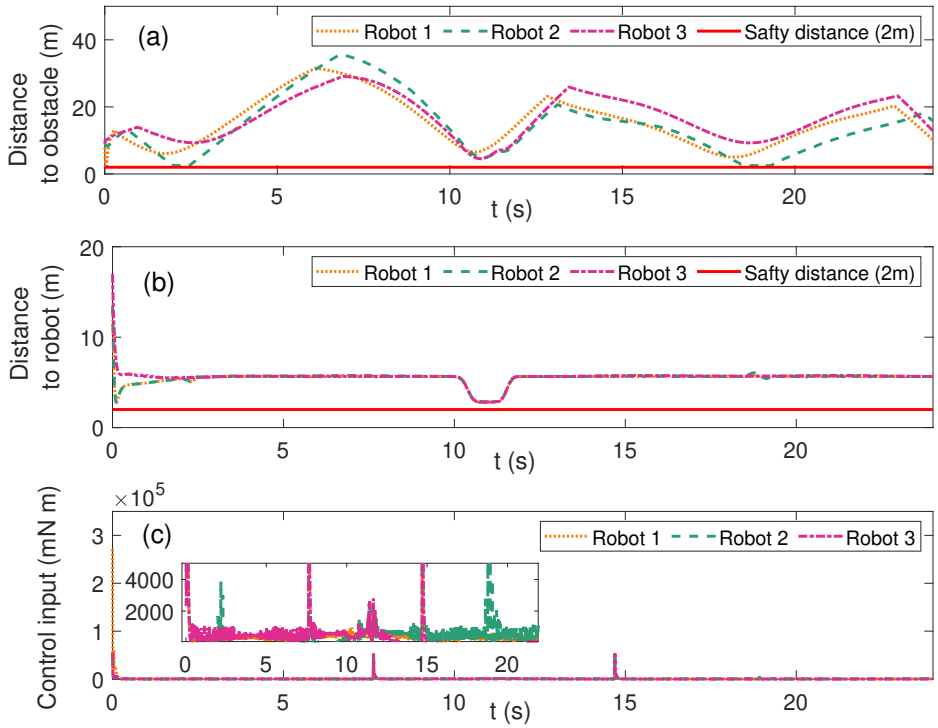

Figure 6. (a) The detected distance between robots and obstacles; (b) The detected distance among the OMRs themselves; (c) The norm of control input.

Multi-OMRs is achieved at both the kinematic and dynamic levels, demonstrating the effectiveness of the proposed scheme. In summary, the proposed fully actuated behavioral control strategy effectively facilitates cooperative behavior decision-making and ensures the precise execution of nonlinear control commands.

5. Conclusion

This paper addresses the collision-free formation control problem for a group of OMRs subject to uncertain dynamics and external disturbances. To solve this issue, a fully actuated behavioral control scheme is proposed, integrating fully actuated system theory with the null-space-based behavioral control method. Initially, three distributed formation behaviors are developed by transforming behavioral functions into a fully actuated configuration. The asymptotic stability of these behaviors and their null-space-based projection fusion is rigorously analyzed. Moreover, a fully actuated sliding mode controller is designed for the over-actuated OMRs, ensuring asymptotic convergence at the dynamic level. This allows for precise tracking of desired kinematic commands in the task space despite model uncertainty. Finally, simulation results validate the asymptotic stability of the closed-loop system, demonstrating the effectiveness of the proposed control scheme.

Disclosure statement

No potential conflict of interest was reported by the authors.

Data availability statement

The authors confirm that the data supporting the findings of this study are available within the article.

Funding

This work was supported in part by the Science Center Program of the National Natural Science Foundation of China under Grant 62188101; in part by the Regional Joint Foundation of Guangdong Province of China under Grant 2023A1515110743; in part by the Natural Science Foundation of Guangdong Province of China under Grant 2023A1515011466; in part by the Guangdong Province Pearl River Leading Talents Program under Grant 2021CX02G450.

Notes on contributor

Zhibin Mo received the B.S. degree from the Department of Engineering, Shantou University, Guangdong, China, in 2018, the M.S. degree in Control Theory and Operations Research from the Fuzhou university, Fujian, China, in 2023. He is currently pursuing the Ph.D. degree in Electronic Information Engineering at Sun Yat-sen University, Guangzhou, China. His research interests include fully actuated control, autonomous mobile robots, and multi-agent system.

Wanquan Liu received the B.S. degree in Applied Mathematics from Qufu Normal University, Jining, China, in 1985, the M.Eng. degree in Control Theory and Operations Research from the Chinese Academy of Sciences, Beijing, China, in 1988, and the Ph.D. degree in Electrical Engineering from Shanghai Jiao Tong University, Shanghai, China, in 1993. He held the ARC Fellowship, the U2000 Fellowship, and the JSPS

Fellowship, and received research funding from various sources totaling over 2 million dollars. He was an Associate Professor in the Department of Computing at Curtin University, Perth, WA, Australia. He is currently a Professor in the School of Intelligent Systems Engineering at Sun Yat-sen University, Guangzhou, China. His current research interests include fully actuated control, large-scale pattern recognition, signal processing, machine learning, and control systems.

Yu-Yao Wu received the B.Eng. degree in Automation from the Harbin Engineering University, Harbin, China, in 2017, and the M.Eng. and Ph.D. degrees in Control Science and Engineering from the Harbin Institute of Technology (Shenzhen), Shenzhen, China, in 2018 and 2022, respectively. She is currently a Postdoctoral Researcher at Sun Yat-sen University, Guangzhou, China. Her research interests include fully actuated control, predefined-time control, and attitude control of spacecraft.

Hui-Jie Sun received the B.Eng. degree in Automation from the Harbin Institute of Technology, Harbin, China, in July 2011, and the M.Eng. and Ph.D. degrees in Control Science and Engineering from the Harbin Institute of Technology (Shenzhen), Shenzhen, China, in January 2014 and September 2018, respectively. He was a Postdoctoral Researcher at the School of Electronics and Information Engineering, Harbin Institute of Technology (Shenzhen), from December 2018 to November 2020. He was a Postdoctoral Researcher at the School of Electronics and Information Engineering, Harbin Institute of Technology (Shenzhen), from December 2018 to November 2020. He is currently an Associate Professor at the School of Aeronautics and Astronautics, Sun Yat-sen University, Guangzhou, China. His research interests include fully actuated control, switched systems, spacecraft control, intelligent systems, and iterative algorithms.

References

Antonelli, G., & Chiaverini, S. (2006). Kinematic control of platoons of autonomous vehicles. *IEEE Transactions on Robotics*, *22*(6), 1285–1292.

Baizid, K., Giglio, G., Pierri, F., Trujillo, M., & Antonelli, G. (2017). Behavioral control of unmanned aerial vehicle manipulator systems. *Autonomous Robots*, *41*(5), 1203–1220.

Bayar, G., & Ozturk, S. (2020). Investigation of the effects of contact forces acting on rollers of a mecanum wheeled robot. *Mechatronics*, *72*, 102467.

Costa, P. J., Moreira, N., Campos, D., Gonçalves, J., Lima, J., & Costa, P. L. (2016). Localization and navigation of an omnidirectional mobile robot: The robot@factory case study. *IEEE Revista Iberoamericana de Tecnologias del Aprendizaje*, *11*(1), 1-9.

Duan, G. (2021a). High-order fully actuated system approaches: Part II. generalized strict-feedback systems. *International Journal of Systems Science*, *52*(3), 437–454.

Duan, G. (2021b). High-order fully actuated system approaches: Part III. robust control and high-order backstepping. *International Journal of Systems Science*, *52*(5), 952–971.

Duan, G. (2021c). High-order fully actuated system approaches: Part I. models and basic procedure. *International Journal of Systems Science*, *52*(2), 422–435.

Duan, G. (2021d). High-order fully actuated system approaches: Part IV. adaptive control and high-order backstepping. *International Journal of Systems Science*, *52*(5), 972–989.

Duan, G. (2024). Fully actuated system approach for control: An overview. *IEEE Transactions on Cybernetics*, *54*(12), 7285-7306.

Duan, G., Zhou, B., & Yang, X. (2024). Fully actuated system theory and applications: new developments in 2023. *International Journal of Systems Science*, *55*(12), 2419–2420.

Eyuboglu, M., & Atali, G. (2023). A novel collaborative path planning algorithm for 3-wheel omnidirectional autonomous mobile robot. *Robotics and Autonomous Systems*, *169*, 104527.

Giurgiu, T., Bârsan, G., Virca, I., & Pupăză, C. (2022). Mecanum wheeled platforms for special applications. In *International conference knowledge-based organization* (pp. 44–51).

Guo, Z., Yee, R. B., Mun, K.-R., & Yu, H. (2017). Experimental evaluation of a novel robotic hospital bed mover with omni-directional mobility. *Applied Ergonomics*, *65*, 389-397.

Huang, J. (2024). Adaptive output synchronization for a class of uncertain nonlinear multi-agent systems over switching networks. *IEEE Transactions on Automatic Control*, *69*(4), 2645-2651.

Jin, X., Wang, Z., Zhao, J., & Yu, D. (2022). Swarm control for large-scale omnidirectional mobile robots within incremental behavior. *Information Sciences*, *614*, 35–50.

Matouš, J., Pettersen, K. Y., Varagnolo, D., & Paliotta, C. (2024). A distributed nsb algorithm for formation path following. *IEEE Transactions on Control Systems Technology*, 1-16.

Mo, Z., Liu, W., Wu, Y.-Y., & Sun, H.-J. (2024). Fully actuated behavioral control for multiple omnidirectional mobile robots system with uncertain dynamics. In *2024 3rd conference on fully actuated system theory and applications (fasta)* (p. 189-194).

Sun, H.-J., Wu, Y.-Y., & Zhang, J. (2023). A distributed predefined-time attitude coordination control scheme for multiple rigid spacecraft. *Aerospace Science and Technology*, *133*, 108134.

Taheri, H., & Zhao, C. X. (2020). Omnidirectional mobile robots, mechanisms and navigation approaches. *Mechanism and Machine Theory*, *153*, 103958.

Takahashi, M., Suzuki, T., Shitamoto, H., Moriguchi, T., & Yoshida, K. (2010). Developing a mobile robot for transport applications in the hospital domain. *Robotics and Autonomous Systems*, *58*(7), 889–899.

Tan, G., Sun, H., Du, L., Zhuang, J., Zou, J., & Wan, L. (2022). Coordinated control of the heterogeneous unmanned surface vehicle swarm based on the distributed null-space-based behavioral approach. *Ocean Engineering*, *266*, 112928.

Thanh, N. T., Long, N. T., Ly, T. T. K., Thai, N. H., & Thien, H. (2023). Dynamics simulation of a mecanum-wheeled omnidirectional mobile robots. In *International conference on engineering research and applications* (pp. 435–449).

Wang, D., Wei, W., Wang, X., Gao, Y., Li, Y., Yu, Q., & Fan, Z. (2022). Formation control of multiple mecanum-wheeled mobile robots with physical constraints and uncertainties. *Applied Intelligence*, 1–20.

Wu, A., Zhou, B., Hou, M., & Zhang, Y. (2022). Fully actuated system approaches: Theory and applications. *Journal of Systems Science and Complexity*, *35*(2), 437–440.

Xiao, H., Yu, D., & Chen, C. P. (2022). Self-triggered-organized mecanum-wheeled robots consensus system using model predictive based protocol. *Information Sciences*, *590*, 45–59.

Yu, D., Chen, C. P., & Xu, H. (2021). Fuzzy swarm control based on sliding-mode strategy with self-organized omnidirectional mobile robots system. *IEEE Transactions on Systems, Man, and Cybernetics: Systems*, *52*(4), 2262–2274.

Zheng, C.-B., Pang, Z.-H., Wang, J.-X., Sun, J., Liu, G.-P., & Han, Q.-L. (2023). Null-space-based time-varying formation control of uncertain nonlinear second-order multiagent systems with collision avoidance. *IEEE Transactions on Industrial Electronics*, *70*(10), 10476-10485.

Zhou, N., Cheng, X., Sun, Z., & Xia, Y. (2022). Fixed-time cooperative behavioral control for networked autonomous agents with second-order nonlinear dynamics. *IEEE Transactions on Cybernetics*, *52*(9), 9504-9518.

Zhou, N., Cheng, X., Xia, Y., & Liu, Y. (2020). Distributed formation control of multi-robot systems: A fixed-time behavioral approach. In *2020 59th ieee conference on decision and control (cdc)* (p. 4017-4022).